Low temperature structural transformations on the (001) surface of $SrTiO_3$ single crystals

N. V. Krainyukova[1], V. O. Hamalii[1], A. V. Peschanskii[1], A. I. Popov[2] and E. A. Kotomin[2]

[1]*B.Verkin Institute for Low Temperature Physics and Engineering of NAS of Ukraine, 47 Nauky ave., Kharkiv 61103, Ukraine*

[2]*Institute of Solid State Physics, University of Latvia, Kengaraga St. 8, Riga LV-1063, Latvia*

Email: krainyukova@ilt.kharkov.ua

Abstract

The smooth (001) surfaces of $SrTiO_3$ (STO) single crystals were investigated by the reflection high–energy electron diffraction (RHEED) method in the temperature range from 5.5 to 300 K. The Raman scattering confirmed the high quality of STO samples. Five structural anomalies were found depending on temperature. The antiferrodistortive phase transition from the cubic structure to tetragonal observed in the STO bulk at 105 K on the surface extends from 70 to 120 K. The anomalies below 7K and about 35K are similar to those in the bulk considered as a crossover between the growth of the ferroelectric atomic displacements with decreasing temperature and quantum–mechanical stabilization of this growth due to the zero–point atomic motion. The other two anomalies are related only to a surface. The comprehensive understanding of the structural properties of ABO_3 perovskite surfaces is important for elucidating the nature of the intriguing effects at the boundary of metallic ferromagnetism in similar materials. Differentiation of lattice parameters depending on the depth from a surface revealed nonmonotonic changes, which could be used for detecting the structural transformations.

Keywords: strontium titanate, surface structural transformations, reflection high–energy electron diffraction (RHEED), Raman spectroscopy

1. Introduction

Perovskites of the ABO_3 type are widely used in many areas of science and technology. In particular, $LaSrO_3$ doped with Sr and more complex (La, Sr) $CoFeO_3$ are used in fuel cells that convert the chemical energy into electricity. $SrTiO_3$ (STO) is an important optical material that simulates diamond, whereas after doping due to its mixed conductivity is used in varistors. Particularly important are its surfaces: STO thin films are used in well–controlled high–temperature superconducting microwave filters, as substrates for epitaxial growth of high–temperature superconductors and many thin films in catalysis. It is commonly known that perovskites with the high dielectric constant ε (in particular STO) have considerable technological potential to be used as high–capacity memory drives such as dynamic random access memories (DRAMs). Such drives are usually made in the form of thin films with a significant contribution of the surface to their behavior.

The most prominent feature of strontium titanate, which distinguishes it among many other perovskites, is the fact that it is a so–called incipient or virtual ferroelectric, but remains paraelectric even when approaching T = 0. Indeed bulk STO exhibits high static dielectric constant even at room temperatures (~300 K), which increases by about two orders of magnitude at 4 K and reaches ~23000 [1]. However, the phonon mode responsible for this typical ferroelectric behavior does not condense at any temperature T down to 0.035 K due to quantum fluctuations that makes STO an incipient ferroelectric with a critical temperature T_c~32 K [1–4]. These experiments proved that the dynamic impulses suppress the phase transition due to the undiminished zero atomic motion. The latter has the greater amplitudes as compared with the ferroelectric displacements. However, the ferroelectric phase can be induced in the bulk STO due to the chemical pressure [5]. Moreover STO can become a ferroelectric in the form of ultrathin films with a large surface contribution due to surface effects [5–8].

Surface relaxation of perovskite–like structures generally leads to mutual displacements of anions and cations and, as a consequence, to ferroelectric properties on the surface, as well as to relaxation of surface layers in general [6–8]. Surface ferroelectricity can act as a stimulating, or vice versa, undesirable effect on various epitaxial growth opportunes on the STO surface, which is widely used in microelectronics. It can be also used directly as a kind of a key for reversible switching the local electric field [9–11]. Possible deviations from the bulk positions of subsurface atoms of strontium titanate may relate also to the rotation of titanium–centered oxygen octahedra about the axes [001] normal to the surface, first proposed for the bulk [12–15]. Such rotations occur, for example, in the region of the known phase transition in bulk STO at 105 K, which is associated with the soft antiferrodistortive (AFD) phonon mode.

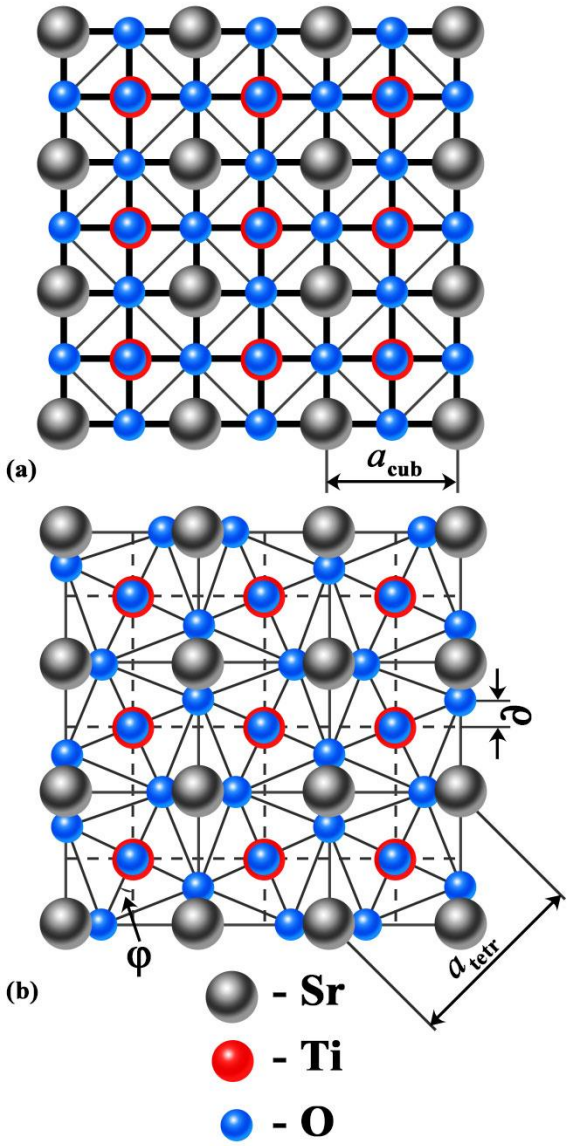

Fig. 1. Atomic structures of the cubic (a) and tetragonal (b) phases of STO. The axis *c* is perpendicular to the figure plane.

The atomic structure of bulk strontium titanate at room temperature was in general defined as typical perovskite [16] with the (pseudo)cubic lattice parameter 3.905 Å. However, accurate X-ray studies performed on high–quality single crystals in combination with optical observations [16] revealed some signs of very small but reproducible deviations from the cubic structure even at the room temperature. The splitting of diffraction reflections about 65 and 35 K, as well as the anomalous behavior of the lattice parameter as a function of temperature at T < 10 K, were initially ascribed [16] to the additional phase transitions, which were not confirmed later, although some almost identical anomalies were observed by other authors [17–20]. Since the deviations from the cubic lattice observed in X–ray experiments were very small, the space group of STO below 105 K was correctly determined only by the electron spin resonance method [12,13,21] as D_{4h}^{18} with two chemical formulas per unit cell. Such a lattice is tetragonal (Fig. 1). The transformation at T_c~105 K was

recognized as a typical second order phase transition associated with the soft mode and the rotation of titanium–centered oxygen octahedra by an angle φ, which causes the displacement δ of oxygen atoms [12–15,22–26]. It is worth to note that a small but clear cooperative motion in the low–temperature phase below 105 K was revealed [12].

The idea of a similar phase transition on a surface has a long history [27,28], but it was robustly confirmed, apparently for the first time, only in Ref. [29] using the ellipsometric measurements on the STO surface. The surface, a very powerful defect, imposes its own symmetry and strongly influences, in particular, the orientations of the oxygen octahedra in the first layers, resulting in rotations and surface reconstruction (and therefore surface properties) very different from the bulk behavior. Determining a complete set of the atomic positions on a surface is a difficult task, and it can be resolved, in principle, by analyzing the high–energy electron diffraction intensities as a function of the electron scattering angle and comparing experimental data with the results of theoretical calculations [30–36].

Thus, structural studies of bulk strontium titanate are quite controversial. Therefore, an additional impetus for the proposed surface study was the potential possibility to find out, which of the three–dimensional (bulk) observations are reproducible on the STO surface as well, but which may be incidental and can be explained by insufficiently controlled experimental conditions.

2. Low temperature RHEED experiment

In this work, we applied the reflection high–energy electron diffraction (RHEED) method to study the structure of the smooth (001) STO surfaces. The special helium cryostat (Fig. 2) joined with the EMR–100 electron diffraction setup was used for experiments in the temperature range 5.5 – 300 K. The high voltage (50 keV) applied at the top of this setup was used to form the thin high–energy electron beam, which further intersects a sample in the center of the vacuum column. The diffraction patterns are formed at the bottom of the column and then recorded either as digital files to a computer or are taken on photographic plates. The second method prevailed in this work.

This combination of the low–temperature cryostat with the RHEED setup enabled us not only to perform measurements at low temperatures, but also allowed attaining the necessary vacuum conditions (better than 10^{-9} Torr) to protect surfaces from undesirable contaminations, which are possible owing to condensation of gases at low temperatures. Such contaminations can affect not only the quality of the diffraction images but also the surface STO characteristics. The temperature of the specimens was varied using the heater Q and measured with the thermometer T. To attain a better

vacuum, the cryogenic trap shown in Fig. 2 at the bottom was applied. Thus, we were able to study the STO surfaces over the wide temperature range from room to liquid helium temperatures.

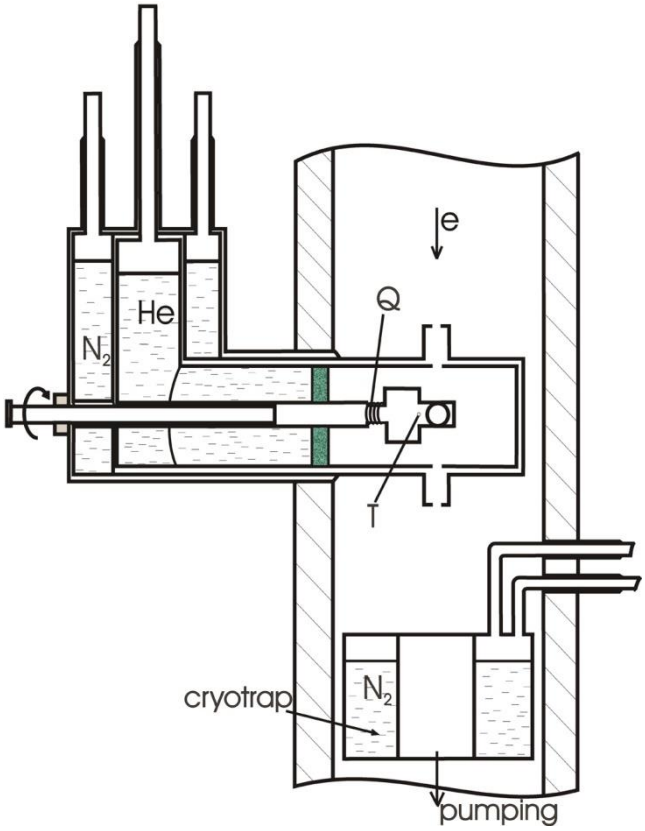

Fig. 2. Special helium cryostat joined to the EMR-100 electron diffraction setup used for the low–temperature experimental studies of STO surfaces.

Fig. 3. The sample of strontium titanate with an atomically smooth surface used in this work for the RHEED and Raman scattering studies.

The experiments were carried out on specially prepared single crystalline samples with atomically smooth surfaces (Fig. 3). There are quite stringent requirements to the quality of the specimens and surfaces being studied. Indeed, such surfaces should be almost perfect and atomically smooth. In our study we repeated the preparation procedure proposed [37], i.e. samples of strontium

titanate (Fig. 3) were first cut from high quality single crystalline blocks, and then they were polished by the chemical–mechanical method using ultrasound. In the final step the sample was heated to ~1000° C and stored in an organic solvent atmosphere during pumping to ultrahigh vacuum. Eventually no signs of reconstruction or other signs of structural changes such as additional reflections etc. on the surface were revealed.

An internal reference (an aluminum film of a thickness ~80 Å), firmly attached to the sample holder, was used to ensure sufficient accuracy in determining the lattice parameters. A gap of approximately 1 mm wide was left between the surfaces of the studied STO single crystals to pass the electron beam through.

3. Raman spectra of the STO single crystal

It is well known that the Raman scattering cross section in the bulk significantly varies (by several orders of magnitude), depending on the possible energy resonance of the incident light with the electronic band structure of solids. Since the electronic structure on the surface is different from that in the bulk, under favorable conditions, when the surface resonance states arise, the Raman signal from surface atom vibrations can increase substantially with respect to the bulk one. This simplifies the task of distinguishing the contribution of the surface in the total signal including the bulk contribution. In our study, the Raman spectra of single crystal STO samples were used to determine and control the quality of the samples that is important for reliable interpretation of the obtained structural information. Only chemically clean and well–ordered samples with atomically smooth surface are suitable for the proposed research.

The Raman spectra were taken with 532 nm excitation wavelength from the solid–state Nd:YAG laser with the power 36 mW. The experiments were performed in the quasiback scattering geometry. The angle between the incident light beam and the sample surface plane was ~22.5˚. Accordingly, the angle between the incident beam and the reflected beam was ~45˚. The light scattered by the sample at the angle 90˚ relative to the incident beam was analyzed using the Ramanor U–1000 dual monochromator and was detected by the cooled photomultiplier working in the photon counting mode.

The STO disc of the high optical quality with the diameter ~8 mm and the thickness ~1 mm was used for the present studies (Fig. 3). In Fig. 4 the Raman spectra of STO obtained at 300 K in two different polarization configurations are presented. A detailed comparison with the known data [38,39] showed similarity between our spectra taken at the room temperature and the spectra in previous works. In Fig. 4 the indices V and H correspond to the vertical and horizontal directions of the electric

vector of the incident and scattered light beams (VV is the vertical direction of the electric vector of the incident and scattered light beams, VH is the vertical direction of the electric vector of the incident beam and the horizontal direction of the electric vector of the scattered light beam).

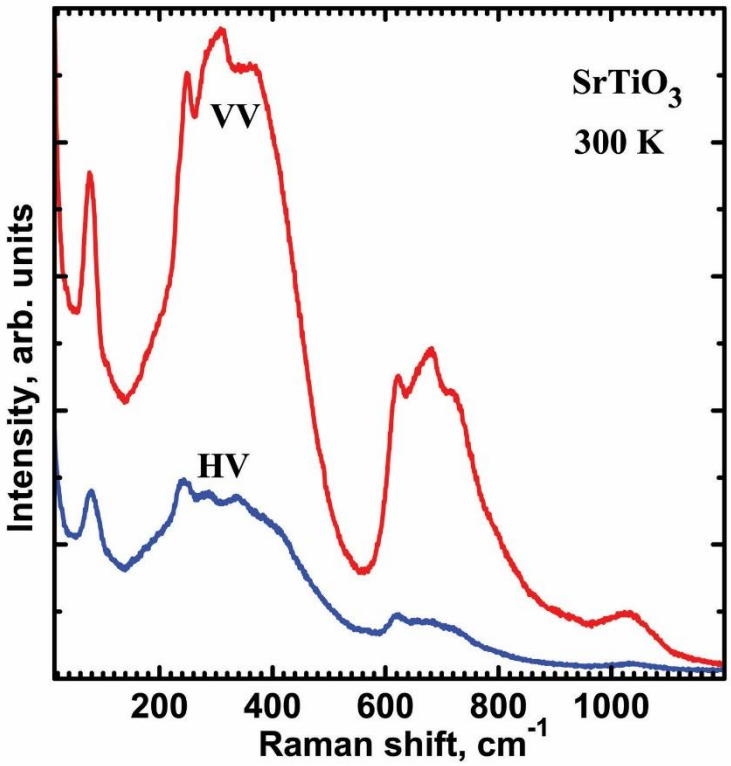

Fig. 4. Raman spectra of the single crystal STO sample at 300 K in two polarization configurations.

It is well known that in the cubic phase of perovskites the first–order spectrum is forbidden by the selection rules in Raman scattering [40]. It is observed however in the tetragonal phase as well as due to presence of domains in the cubic phase. For example, the anisotropic first–order response from a single tetragonal domain was observed by micro–Raman spectroscopy in strontium titanate in its tetragonal phase [41]. We believe that in this study only the second–order spectrum is observed as shown in Fig. 4. This follows from typical for the second order spectra broad and asymmetric Raman lines and similarity with the second–order spectra in the previous studies for the pure STO crystals [38–40]. Indeed, at room temperature, we do observe neither the lines inherent to the low–temperature tetragonal phase nor any additional lines that may be associated with the presence of impurities. Thus, the tested STO samples do not have any detectable defects which can violate the selection rules in the Raman spectra or lead to the appearance of additional lines. Thus we conclude that the tested samples have the good quality and could be used in surface studies.

Below we discuss some details of possible spectra. As mentioned above, the structural AFD phase transition in the STO bulk crystals caused by the softening of the three–degenerate mode at the boundary of the Brillouin zone occurs at T_{tr}~105 K. This transition corresponds to the antiphase

rotations of the titanium–centered oxygen octahedra TiO_6. In STO ceramics the phase transition temperature can be shifted up to ~132 K [39]. Such a difference in T_{tr} most plausibly relate to the internal strains in ceramics. It is known also that the hydrostatic pressure increases T_{tr} in STO. Besides, the small amounts of calcium may also increase T_{tr}. This transition results in the doubling of the unit cell along the rotation axes accompanied with the reduction of the symmetry from cubic to tetragonal ($D_{4h}^{18} - I4/mcm$). As the result of the lattice doubling the phonon branches add to each other and in the Raman spectra formed in the tetragonal phase below T_{tr} new modes appear arising from the boundary of the Brillouin zone: $A_{1g} + 2A_{2g} + 2B_{1g} + B_{2g} + 3E_g$. The above mentioned three–fold degenerate soft mode splits into two components A_{1g} and E_g and also becomes active in the Raman spectrum. Thus the Raman spectrum of STO in the tetragonal phase arises due to phonons from the boundary of the Brillouin zone. Obviously, in ceramics and powders, many symmetry disturbances caused by disorder, vacancies, impurities, pressure, etc., lead to violations of the selection rules in Raman spectra. In films of ferroelectric materials not only violations of the selection rules can be observed, but sometimes a very significant transformation of the phonon spectrum can be found related to the phase symmetry change and the sequence of structural transformations.

4. Two types of the RHEED geometry in the study of STO single crystal surfaces

Two different modes of diffraction imaging both inherent to RHEED were applied to the low–temperature surface studies of STO depending on the tasks described below. One is typical of RHEED, this is the method when shooting is carried out at the fixed angle of electron incidence. In Fig. 5 we show a scheme of experimental shooting in the RHEED method and obtained diffraction images from the surface (001) of strontium titanate at the fixed angle of electron incidence Θ and azimuthal orientation [100] of a sample.

The high–energy (50 keV) electron beam falls on the surface (100) of strontium titanate at very small sliding angles Θ. This allows obtaining information only about 3 – 4 surface layers of a single crystalline structure of STO since the penetration of electrons into a sample is very small. Penetration depth is a function of the angle Θ. Indeed, to the first approximation, the electron free path l in a crystal can be regarded as a constant independent of the reflection angle Θ, and the scattering volume $V = S \cdot \Delta$, where S is the beam irradiated surface (the angle dependent), and Δ is the effective electron penetration depth into the crystal before electron scattering or absorption. In turn $\Delta = l\sin\Theta$, i.e. the smaller is the angle Θ between the electron beam and the surface, the smaller is the depth Δ of electron penetration into the crystal and, accordingly, the contribution from the first surface layers is greater. Therefore, by varying the angle of incidence, we can obtain information either from one surface layer or from several (but no more than 3 – 4 layers in the applied geometry). The RHEED studies at fixed

angles are more common to determine lattice parameters on single crystal surfaces. However, a large number of "dynamic effects" such as the Kikuchi lines and some others can appear in the diffraction pattern at a fixed reflection angle (Fig. 5) often preventing the precise analysis of the data.

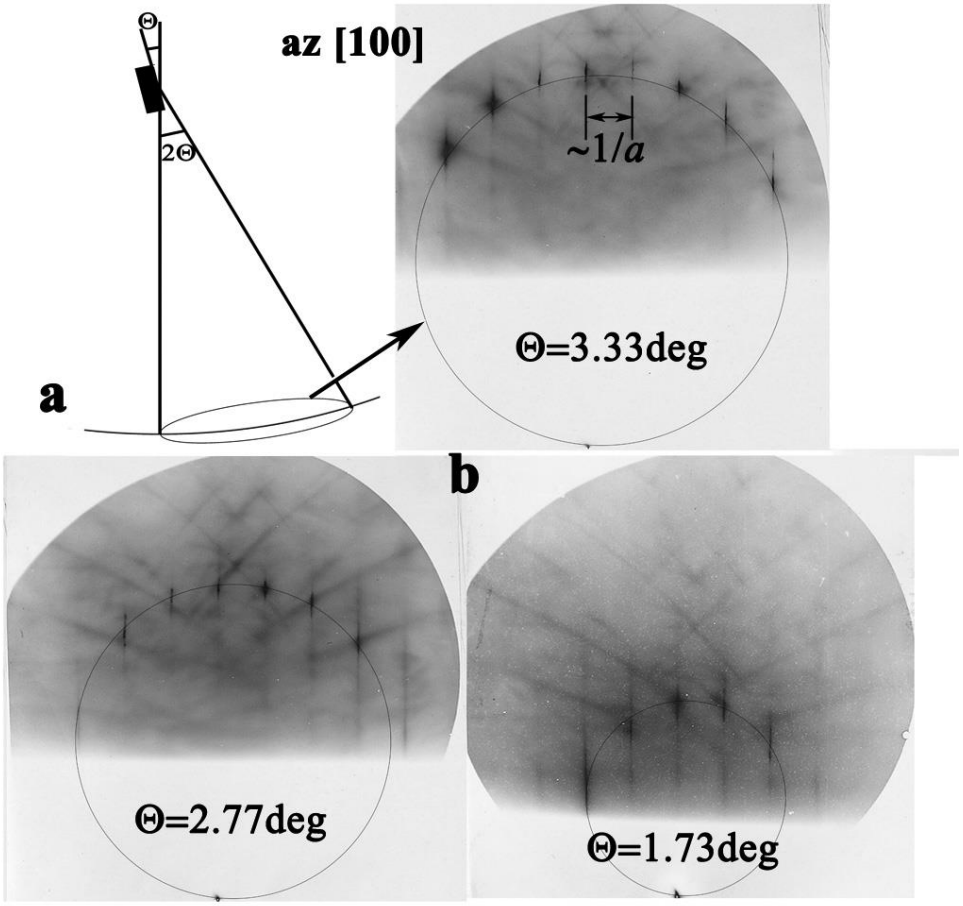

Fig. 5. Experimental scheme of diffraction imaging in the RHEED method (a) and obtained diffraction images from the surface (001) of strontium titanate at the fixed angles Θ of incidence and azimuthal orientations [100] of the samples (b).

The reciprocal lattice of atomically smooth single crystal surfaces is (quasi)two–dimensional and comprises from straight parallel regularly arranged rods, perpendicular to the surface and weakly modulated in thickness that takes into account the smaller contributions of the deeper layers. The distances between the rods are inversely proportional to the distances between the planes perpendicular to a surface. In particular, in the case of azimuth [100], these distances are proportional to the parameter *a* of the (quasi)cubic lattice parallel to the surface. The diffraction pattern is the intersection of the rods of the reciprocal lattice and the so–called Ewald spheres, whose radius is inversely proportional to the electron wavelength (~0.055 Å for 50 keV), as shown in Fig. 5. The intersection of the sphere by the plane formed by the system of parallel in–plane rods is a circle.

Dynamic effects such as the Kikuchi lines and some others that appear in the diffraction pattern at the fixed angles Θ "disappear" when we use the another original method of image recording, in

which the angle of incidence changes continuously during exposition (Fig. 6). In this case the rods of the reciprocal lattice intersect the Ewald sphere along the lines whose projections are indeed displayed in the diffraction patterns in the form of straight lines corresponding to the particular rods. In this mode all visible reflections can be explained on the basis of the quasi–kinematic approach applied to the diffraction intensity analysis earlier [42]. Therefore, both fixed–angle and continuously varying angle modes are used in this work depending on the problem being resolved. The second method is more informative because it enables us to capture data pertaining to the different angles of incidence and to different depths of electron penetration into the sample in one record.

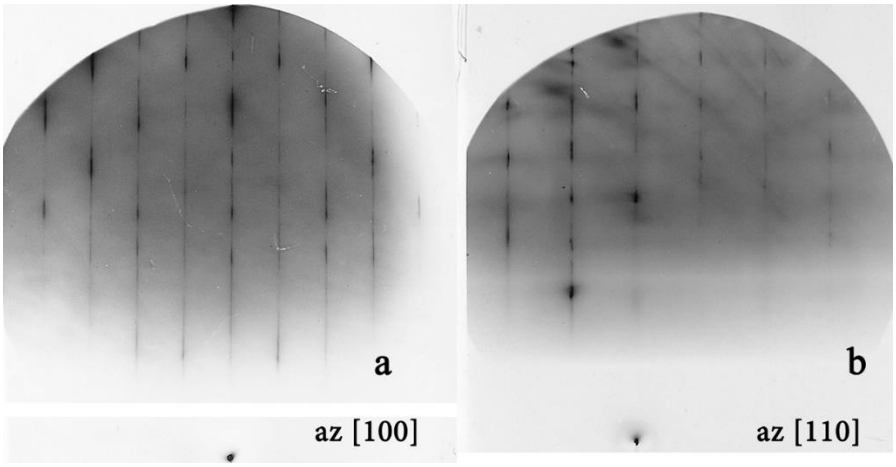

Fig. 6. Diffraction images from the surface (001) of strontium titanate at the continuously variable angle of electron incidence during image recording and azimuthal orientation of the sample [100] (a) and [110] (b).

In a case of the second method, the general procedure for measuring the surface lattice parameters as a function of the angle of electron incidence is as described below. In Fig. 5 we show, along with diffraction images, the circles, each corresponding to the specific angle of incidence of electrons. In this case, the distances between the central rod and the points of the lateral rods intersections with the Ewald sphere related to the same angle of electron incidence are used to determine the surface lattice parameters in the plane parallel to a surface. Such parameters were found in this work to depend on the angle of electron incidence. Similar circles are also used in the second method in application to the images shown in Fig. 6. Then the distance between the nearest intersection points in every circle is roughly inversely proportional to the parameter a of the surface lattice in Fig. 6a, whereas in Fig. 6b such a distance is inversely proportional to the distances d_{110} between the respective planes (110) perpendicular to the surface.

The data analyzed in this work can be compared with the results of the recent study of the STO surface at room temperature by the low–energy electron diffraction (LEED) method [8], in which another but similar electron diffraction technique was used, namely the electron diffraction with

relatively low electron energies. In this case, the diffraction pattern is the intersection of the reciprocal lattice rods with a sphere of small radius, where the central rod coincides with the diameter of the Ewald sphere and the electron beam direction. The scale of the images changes depending on the energy of the electrons applied in this method.

5. Differentiation of lattice parameters values depending on depth from crystal surface

In our previous work [43] we studied the lattice parameters averaged over several surface layers in a plane parallel to the surface, but neither the nature of the observed increase of the lattice parameters in a plane parallel to the surface with the temperature decrease nor the large enough scattering of the data observed were not established. The RHEED geometry is rather complicated, and as it is shown in this paper only differentiation of lattice parameters values depending on the angle Θ may result in the correct lattice parameters. Slight incommesurability between the lattice parameters on a surface in parallel to the surface directions relative to the bulk parameters can be realized due to the small miscut angle ~0.9˚ between the crystallographic plane (100) and the real surface that results in a stepwise surface substructure, as well as due to the surface dislocations of inconsistency. Such imperfections may cause the essential changes of phonon spectra on a surface not only due to surface bond breaking but also owing to surface vacancies as discussed for a similar perovskite $BaZrO_3$ [44] or due to surface relaxation and rumpling effects [6–8,31,32,35].

In this work we first applied differentiation of the lattice parameters as a function of the layer number from the surface that revealed the nonmonotonic character of changes of such parameters deeper into the crystal in some temperature intervals that could be explained by the competition of the contributions of TiO_2 and SrO layers as well as by the broken surface symmetry. The depth of electron penetration into the crystal depends on the angle Θ of incidence. Indeed for very small Θ the probability of electron penetration to the deeper layers is almost impossible since the atoms have finite dimensions and the scattering occurs only in the first 2–3 layers since these upper layers screen electron penetration deeper.

The maximum (or minimum) lattice parameter value is reached on the surface, while further monotone or nonmonotonic changes of parameters are observed in particular temperature intervals. Perhaps this effect at least partly depends on whether the contribution from the TiO_2 or SrO layers are added to the overall diffraction pattern when electrons penetrate deeper into the scattering crystal. Indeed, in the (001) plane formed by TiO_2 with the central part of the oxygen octahedron undergoing significant reversals by several degrees, the parameters may be larger than those in SrO layers with almost fixed positions of oxygen atoms. In general, theoretical studies show that the rotations of

oxygen octahedra on TiO_2 surface are smaller than those in the bulk [34]. This may explain the smaller values of the lattice parameter in the first layer compared to the deeper layers in the temperature intervals, where no structural transformations occur, although the other reason could be the broken surface symmetry. On contrary, when the structural transformation occurs, the lattice parameters in the first surface layer typically take maximum values that will be described and discussed in detail in the following section. Thus, it can be concluded, at least empirically, that a significant increase in the lattice parameter in the first surface layer can be considered as an indicator of the structural transformation.

6. Structural transformations on the surface as a function of temperature

We report in this paper several structural transformations on the surface (001) of STO samples depending on temperature, which only partially correlate with the known bulk data. In Fig. 7 we present a general view of the data to illustrate the character of the surface lattice parameter dependence on temperature, measured in a plane parallel to the surface over the entire temperature range studied.

Using the smaller incidence angles in the 0.7–1.3 (1.4) deg range, we can obtain the diffraction image only from the first surface layer, whereas the larger incidence angles accordingly make the electron penetration depth into the crystal higher. Thus, in the range of angles of 1.8–2.5 deg it becomes possible to obtain information not only from one but at least from two surface layers, and the further increase of Θ to values 3.3–4.0 deg opens access to the third and perhaps in part even to fourth layers.

As it is clearly demonstrated in Fig. 7, in general one can distinguish five separate temperature intervals in which different structural transformations were observed in our experiment. These intervals are marked and numbered in Fig. 7 for convenience of description and references. It is likely that structural transformations on the surface are not rigidly bound to any fixed temperature points because several surface layers (but not only one) are not equivalent in terms of symmetry and interatomic interaction. Therefore, it is natural to assume that any transformation begins in the first layer and also ends at different temperatures compared to the second or third layers. Therefore, instead of the fixed temperature points, we should consider structural transformations in the temperature intervals. However, it looks likely that most transformations are still spaced in temperature and separated from each other. The largest incidence angles achieved in our diffraction experiments are 3.5–4 deg. For such small angles, the depth of electron penetration into a crystal is according to our estimation equal or less than 3–4 layers, and indeed in such experimental geometry we obtain

information only from the surface. Further we consider in detail each of the observed structural transformations.

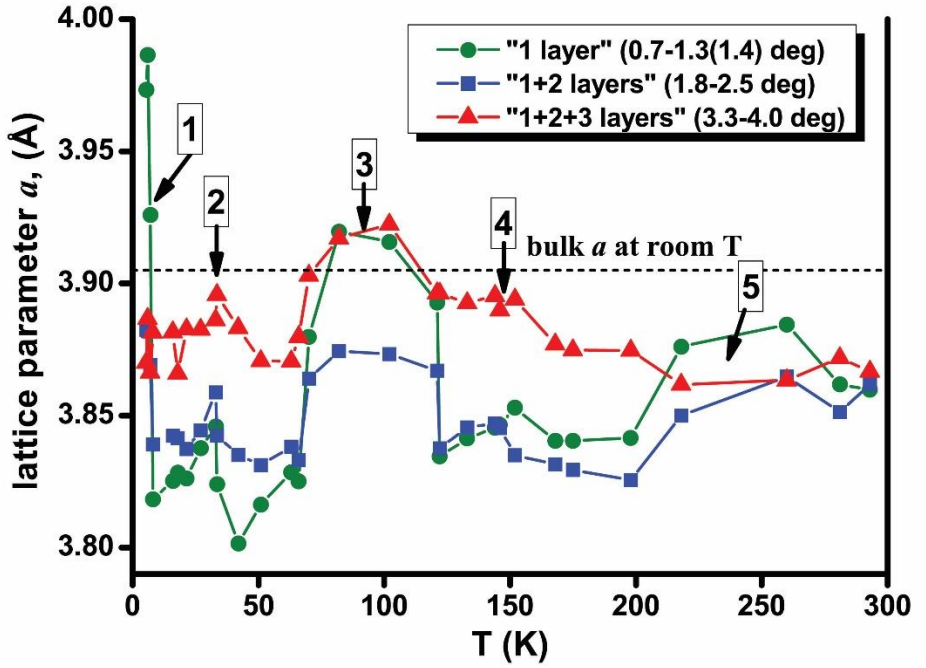

Fig. 7. Dependence of the lattice parameters parallel to the surface (100) STO on the temperature. Using circles, squares, and triangles, we distinguish the data relating solely to the first surface layer, to a mixture of the first and second layers and the averaged data over the three surface layers, respectively.

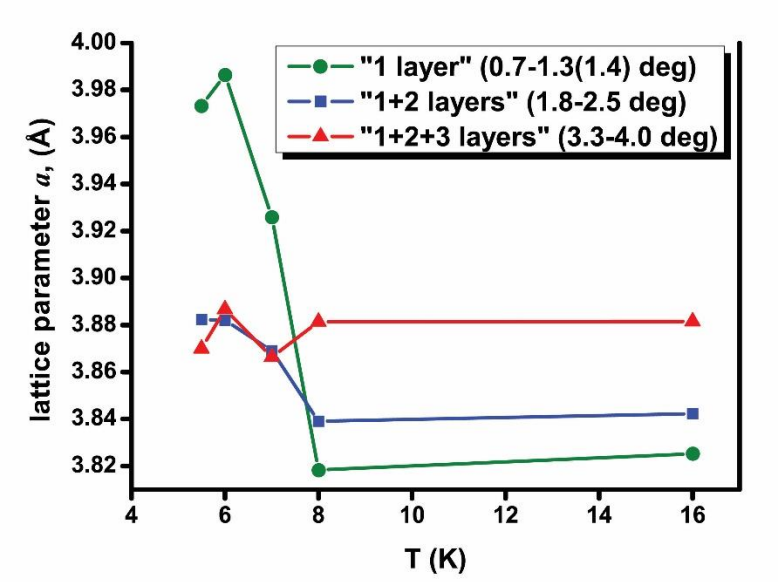

Fig. 8. Dependence of the surface lattice parameters when approaching T=0. The abnormal and highest increase of the parameter occurs in the first layer on the surface, the averaged values over the first and second layers are lower, while no significant changes are observed in averaging over the three layers.

In our experimental study, the abnormally high increase of the lattice parameter in the first surface layer was observed at the temperatures below 8 K (Fig. 8). From 6 K the data does not change significally with the further decrease in temperature. On the contrary, at the higher temperatures, i.e. above 8 K, no anomaly in the first layer is observed when heated up to at least 22 K.

In general, the structural changes seem to occur only in the first surface layer, and when averaging the lattice parameters over the first and second layers, the parameter increase is most likely due to the first layer. This behavior suggests that in a zone of active structural restructuring the transformations begin from the surface. Therefore, the question remains open, whether structural transformations in the deeper layers of a crystal can occur with the further temperature decrease, or the largest anomaly in our study applies only to the first surface layer. More research at temperatures below 5 K is needed to find the answer.

More details are seen in Fig. 9 for the lattice parameter changes on the STO surface as the function of temperature and also differentiation of their values depending on the depth from the surface. This figure shows the dependences of the surface lattice parameters on the angle of electron incidence. The experimental results shown in this figure below 7 K as well as above 8 K and up to at least 22 K are reproduced fairly well. However, there are radical changes between these two temperature points in the behavior of the lattice parameters, which are the most significant in the first two surface layers ($0.7<\Theta<2.5$ deg). As concerns this observation, we should certainly recall the fact that the quantum–mechanical stabilization of the paraelectric phase occurs below 4 K. Further research is needed to determine whether the observed anomalies relate to the bulk behaviour discussed also below or are specific to surfaces only.

As it was already discussed above, in many aspects the behavior of strontium titanate differs from that in typical paraelectrics. In bulk STO the high static dielectric constant is observed even at room temperatures as it occurs in many ferroelectrics. This constant gradually increases at lowereing temperatures and at 4 K reaches ~23000 [1]. This actually means that ferroelectric transformation almost occurs in STO at low temperatures. This at first provoked the expectation that eventually this ferroelectric transition could be reached if the temperature would be low enough. However, as it was found later [1], the phonon mode associated with this typical ferroelectric manifestation does not condense at any temperature down to 0.035 K. This behavior is explained by the quantum–mechanical stabilization of the paraelectric phase below 4 K and may result in a crossover from classical to quantum behavior when the temperature is lowered and the ferroelectric mode attaches to the acoustic one [1–4]. Below 4 K the quantum–mechanical mode stabilizes large ferroelectric oscillations of the wave vector $q = 0$ in the paraelectric phase. In other words, the presence of a dynamic impulse suppresses the phase transition.

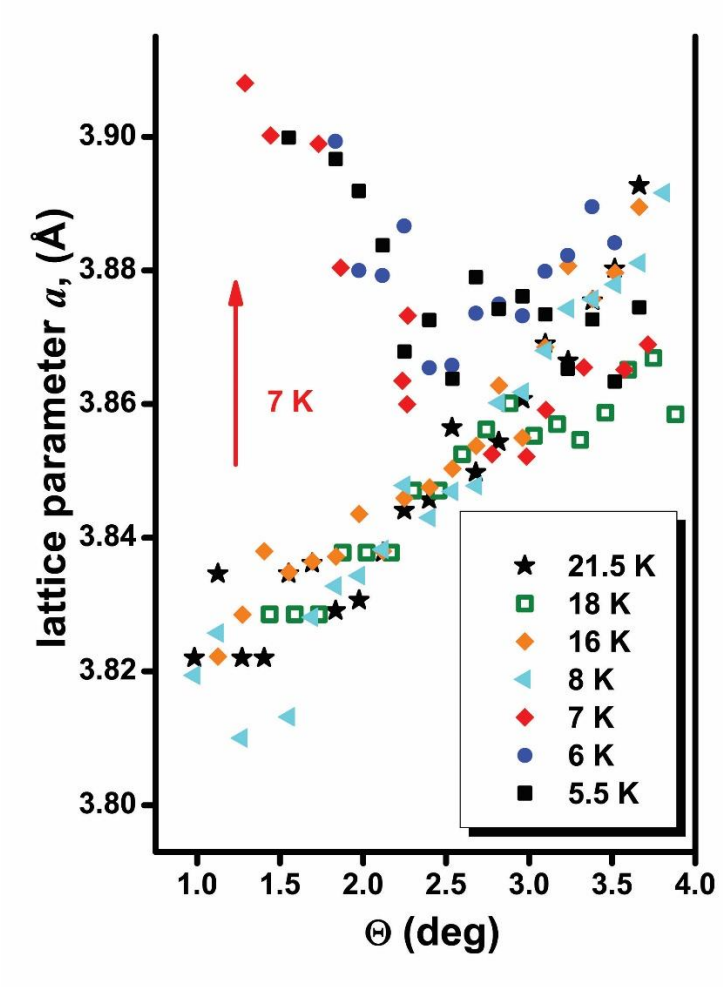

Fig. 9. Illustration of an abnormally high increase in the lattice parameter in first two surface layers observable at the angle of electron incidence $0.7<\Theta<2.5$ deg when T decreases below 7 K.

There were some debates in the literature whether the theory, well developed for the critical behavior of ferromagnets, could also be applied to ferroelectrics near the point of the expected transition to the ferroelectric phase. In the recent paper [45], to answer this question, the temperature dependence of the dielectric function in two quantum paraelectrics STO and $KTaO_3$ was investigated. In the case of STO, the samples with the oxygen substitution with the ^{18}O isotope were also analyzed. For all these objects the nonclassical dependence T^2 of the inverse dielectric function below 50 K was observed, which ended with anomalous growth below a few kelvins and down to the millikelvin zone. It is argued that such non–classical behavior can be understood even quantitatively without additional fitting parameters within the theory of the critical behavior if the long–range dipole interaction and the bonding of the electric polarizing fields with acoustic phonons will be added to such a theory. Thus the quantum–critical regime in ferroelectrics with atomic displacements is very different from that in the ferromagnetic analogues that opens up unexpected prospects in the field of quantum phase transitions.

The quantum–mechanical stabilization of the paraelectric phase discussed above first was predicted below the critical temperature $T_c \approx 35$ K. However, as it was found later in the experimental

studies [1–4], the role of the phonon mode connected with the ferroelectric behaviour becomes significant only below 4 K. The next anomaly in our study with the number 2 in general Fig. 7 was also observed close to ~35 K. The noticeable increase in the surface parameters occurred in all three surface layers that indicates the possible bulk behavior. The further research is required, to elucidate if it is really true. However, one significant feature observed in this temperature range deserves our attention right now. In the study [16] there were found the structural changes in this T range, which behave differently under heating and cooling, i.e. the hysteresis in the behavior of the bulk lattice parameter in this temperature range was clearly demonstrated. The hysteresis is often interpreted as manifestation of ferroelectricity in the objects under study. In Fig. 10 we show the hysteresis effect in the temperature dependence of the lattice parameter on the surface, which can be mainly attributed to the second surface layer (Θ~1.8–2.2 deg).

The behavior of the dielectric constant in perovskites is very important because ferroelectrics with high constant are widely used as high–capacity memory drives such as dynamic random access memories (DRAMs) [46]. However, such drives are used in the form of thin films, whose properties are determined in a large degree by significant contribution of a surface. As it was revealed through direct measurements, the dielectric constant decreases significally in thin films compared to bulk crystals. This observation crucially reduces the potential of such materials to be used as storage units. Additional studies had resulted in conclusion that the dielectric constant decrease owes to the presence of a so-called “dead layer” with a very small dielectric constant between the ferroelectric film and the electrode. Since only a few direct measurements of the “dead layer” effect were available, it was later established in independent experiments [46] that the dynamic properties of the crystal lattice (rather than the “dead layer”) play a key role in reducing the dielectric constant. Spectroscopic ellipsometric studies in the far infrared range as well as low frequency dielectric constant measurements reported in [46] showed that the typical Lyddane–Sachs–Teller relation between the optical–phonon eigenfrequencies and the dielectric constant in STO thin films are the same as in a bulk material. This means that the dramatic decrease in the dielectric constant is a consequence of fundamental changes in the dynamic properties of the lattice, in particular, the reduced softening of its lowest optical–phonon mode. In other words, these observations resulted in conclusion about hardening the soft modes in the films resulted in the drop of ε. This observation was fundamental to understanding the limitations of the magnitude of the dielectric constant in thin films. The eigenfrequencies of the higher optical modes, as stated in Ref. [46], do not experience any variation depending on the crystal size, and in bulk STO a dramatic increase in the dielectric constant occurs only due to the behavior of the soft mode.

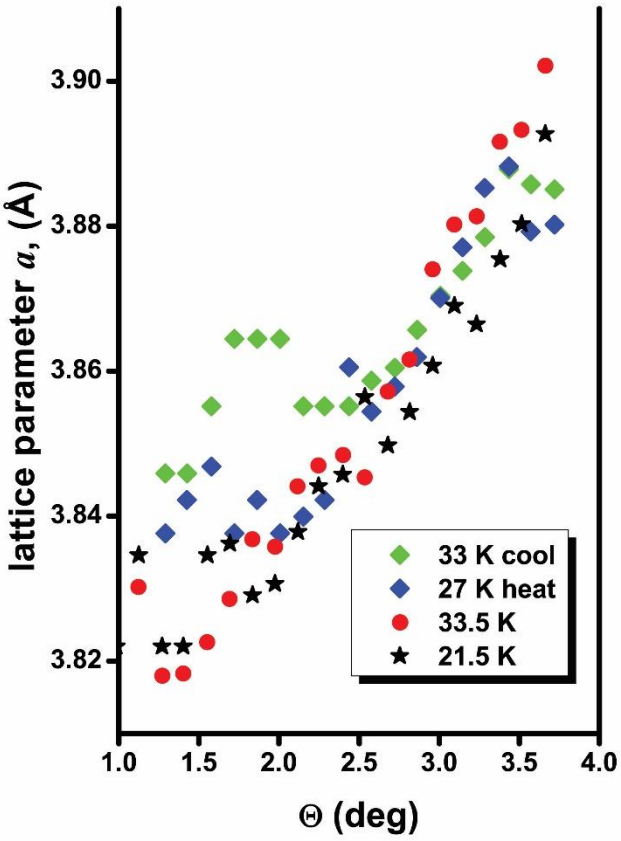

Fig. 10. The dependence of the surface lattice parameter on the electron incidence angle in the temperature range 21.5–33 K. Comparison of the dependences obtained at 33 K during cooling and at 27 K when a sample was heated indicates hysteresis.

We have to admit here that at least two key points are missed in the above discussed studies. First, we have to note that the hardening of the soft modes may be caused by the size effect in small STO crystallites in thin films. Indeed, in nanocrystals the phonon wave length is limited by the crystallite sizes, and therefore the long wave length modes are forbidden. The second point concerns the stoichiometry of samples. If samples are far from perfect, one may expect that some limited conductivity may arise and reduce the dielectric constant as well. Summarizing this discussion, we must conclude that additional studies, both experimental and theoretical, are necessary, to find out what actually happens at the lowest temperatures with the dielectric constant, atomic structure, and dynamic properties of STO atoms in thin films versus the bulk behaviour, while the properties of thin films are inherently related to the surface of a crystal. If films could preserve the single crystal structure even with small thickness, we may expect also at leats two–dimensional infinity of phonon mode lengths that therefore may open an additional opportune for the higher dielectric constant in such films. Both the structure and the dynamics of atoms in STO can be studied by the RHEED method.

The bulk properties of strontium titanate are believed to be well understood, including the known AFD phase transition below 105 K from the cubic structure to the tetragonal phase (Fig. 1)

[12,13,21,23]. This transition is one of the most pronounced bulk effects in STO, which as above discussed is not ferroelectric and remains a quantum paraelectric at non–zero temperatures. This transition owes to softening the phonon modes and leads to doubling the unit cell size (with two chemical formulas per a cell) along the *z* direction (normal to the surface) with the alternating rotations of nearby TiO_6 octahedra in opposite directions. Accordingly, the cubic space group 221 ($Pm\bar{3}m$) is replaced by the tetragonal space group 140 (I4/mcm). As discussed above, phonons play an important role in the phase transitions in perovskite titanates. The eigenfrequencies of the lowest optical mode (the soft mode) fall as the temperature decreases and were expected to approach zero at the critical temperature that could lead to the lattice instability and the ferroelectric phase transition. The Landau theory and the analysis using the group theory indicated that the observed phase transition is caused by the softening of the R_{4+} phonon mode. This result was successfully reproduced in Ref. [35] where the theoretical consideration based on first principles calculations was applied.

The idea of the AFD phase transition on the surface as well as in thin films of STO similar to those observed in the bulk has a long history. Three directions [100], [010] and [001] are equivalent in the bulk but the surface anisotropy with different interactions in the normal and parallel directions relative to the surface plane makes one of three directions different with respect to two others on the surface and causes in particular the differences in rotations of metal–centered oxygen octahedra about the axes *a* oriented along the [100] and [010] directions and about the axis *c* oriented along [001]. Indeed, in Fig. 11 we show the strong structural transformations occuring at the surface close to ~100 K (the anomaly 3 in Fig. 7).

However, in contrast to the bulk, this transformation on the surface turns out not to be localized at a fixed temperature but extends over the temperature interval. If the phase transition from the cubic to tetragonal structures is realized in the bulk of STO about 105 K and as mentioned above is associated with the AFD soft phonon mode, then a similar structural transformation on the surface extends over the temperature range from 120 K down to 70 K. According to our observation, this transition begins at 120 K from the strong increase of the lattice parameter in the first and possibly (to a lesser extent) in the second layers on the surface (Fig. 11) whereas the transformations in the deeper layers are shifted to lower temperatures. Also, this transformation ends only around 70 K, where the surface lattice parameter in the first layer also changes last. These observations confirm our two initial assumptions, firstly, that phase transformation begins (and also ends) with an increase in the lattice parameter in the first surface layer, and, secondly, that surface phase transitions that propagate in the bulk do not occur at the given fixed temperature but extend over the temperature interval. This implies that the transformation gradually layer by layer penetrates deeper into a crystal as the temperature changes.

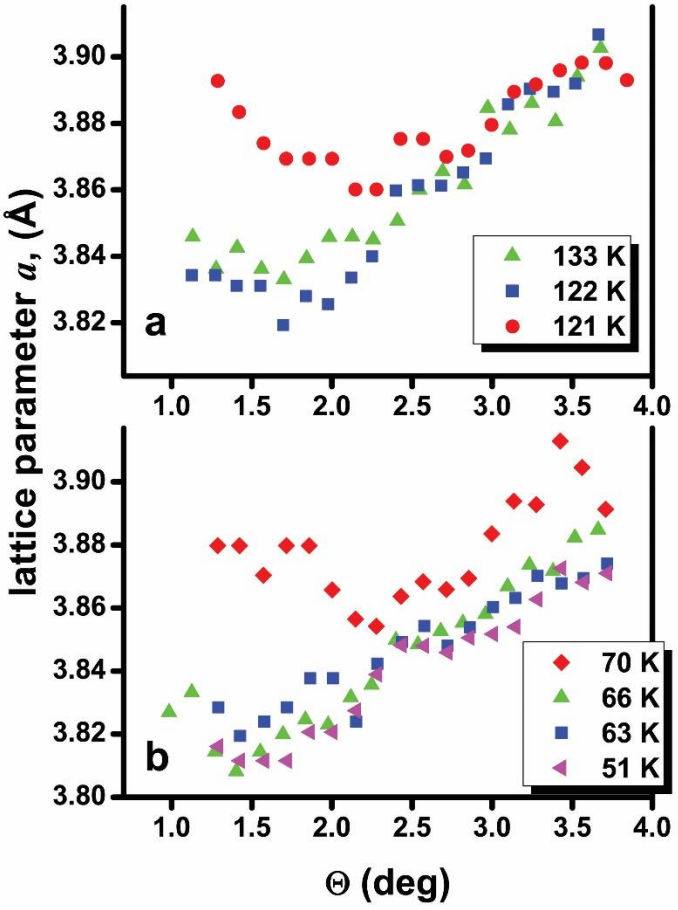

Fig. 11. The surface lattice parameters as the function of the electron incidence angle on the STO surface or (that is the same) on the depth of electron penetration into a crystal at the beginning at ~120 K of the phase transition, which is likely to be of the same AFD type as in the bulk at T≈105 K, at decreasing temperatures (a) and at the end of the structural transformations at ~70 K (b).

As it is evident from Fig. 7, the variety of structural transformations that occurs on the surface of strontium titanate is not limited by the changes in the structures discussed above, which highly plausible are related to the bulk transitions. So, there is a rather noticeable anomaly about 150 K numbered as 4, which arises mainly only in the first two surface layers and possibly only partially and to a lesser extent affects the third layer, which is already close to the bulk in terms of spatial symmetry. This transformation is largely local that indicates the possibility of the two–dimensional phase transition at the surface at these temperatures. At higher temperatures, in the range between 200 and 300 K, an additional transformation with the number 5 in Fig. 7 is noticeable and also occurs only in the first two layers and practically does not affect the third. We have not been able yet to find reports of such transformations at these temperatures in the literature.

Explaining the nature of these transformations requires additional experimental and theoretical efforts, but apparently these structural changes apply almost exclusively to the first two layers of the

STO single crystal. It is likely that the oxygen subsystem can be transformed on the surface that in turn can lead to less significant shifts in the positions of the metal ions. There are several hypothetical possibilities. Firstly, these transformations can probably relate only to restructuring in the oxygen subsystem, for example, by deviations in the stoichiometric oxygen composition, which may in particular result in the appearance of conductive properties on the surface of the 'insulator' STO. Besides, in the LEED study [8] the surface structural distortion quantified by the low–energy electron diffraction method at room temperature was detected. Structural analysis of the data showed that the surface layers are slightly warped or rumpled due to the oxygen atoms shifting outwards and the titanium atoms moving inwards at the TiO_2 surfaces. The relevant DFT calculations [31,32,36] confirmed the measured mutual displacements of surface titanium and oxygen atoms in opposite directions along the *z* axis. Secondly, as in the case of structural transformations at lower temperatures, the titanium–centered oxygen octahedra TiO_6 may be the main elements of the transformations. There are several scenarios in this connection that should be considered in additional experiments and theoretically. The first option is such that the octahedra rotations about the axes normal to the surface may change significally with the temperature causing the anomalous behavior of the surface lattice parameters. Besides the surface defects such as exits of dislocations, vacancies, or surface steps may affect additionally these rotations. Defects due to the incommensurability of the surface lattice with respect to the deeper crystalline layers near the surface should also be considered. One more option is the possibility of tilting the octahedron axes to the surface that should not be excluded. Such slopes can be both random and ordered, and structural transformations may be related to the transitions between the two possibilities.

The surface transformations could be of the more complicated nature. In particular, the fact that the valence of titanium on the surface is increased as compared with the bulk, while the valence of oxygen is weakened, and that the Ti–O chemical bonds are considerably more covalent in comparison with the bulk behavior was experimentally [8] and theoretically [32,36] proved. Another theoretical prediction is considerable change of the phohon spectra in thin films compared to the bulk [35,45,47] and formation of the dipole moment perpendicular to the surface due to atomic relaxation [33]. The experimental data show that all anomalous changes are localized near the surface and do not extend into the depth of a crystal.

The electronic hybridization on a STO (001) surface is the subject of research and interesting discussions in other papers. For example two types of symmetry related to the electron orbitals depending on the displacements on the surface (001) of the STO sample were found by the scanning tunneling microscopy method [48]. The transitions between these types of symmetry were of the tunnel character and well reproduced. In fact, the electronic structure switches forth and back between

two sets of symmetry parameters that is accompanied by non trivial changes in the energy dependent spectroscopic data. The DFT calculations have shown [48] that the symmetry breaking on the surface causes splits in the crystal field of the electron orbitals on the surface while recording images with strong anisotropy in the surface plane. This occurs in such a way that the electrons alternately fill the orbitals corresponding to different types of symmetry in the displacement process along the surface. Such manifestations of the surface superstructure require new approaches, to gain the understanding of the nature of appearance of orbital texture and orbital selectivity on the surface. Note that first principles calculations of the non–cubic perovskite phases need use of the accurate but time–consuming state–of–the–art hybrid functionals since structural transformations are associated with very tiny (several meV) changes of the unit cell energy [30,35], whereas TiO_6 rotation angle is predicted to be as small as ca. 2 deg in the bulk and 1 deg on the surface [30,34].

7. Summary

The low–temperature version of RHEED was implemented for the comprehensive study of the surface lattice parameters of the atomically smooth (001) surface of STO single crystals in the wide temperature range from room to liquid helium temperatures. Raman scattering was applied to confirm the good quality of STO samples.

Five structural anomalies were found, indicating structural transformations on the surface at different temperatures. Some of these anomalies correlate with the known bulk data. At temperatures below 7 K an abnormally high increase in the lattice parameters was observed in the first surface layer that may correlate with the known high growth of the dielectric constant in the bulk at helium temperatures.

There is also an anomaly around 35 K, close to the critical temperature, which is considered in the bulk as the point of the possible crossover between the gradual growth of ferroelectric displacement at decreasing temperatures and the quantum–mechanical stabilization of this growth due to the significant zero atomic motion in a crystal. For this anomaly at 35 K, the hysteresis was observed, i.e. the lattice parameters at heating and cooling differ by a noticeable value.

Unlike the STO bulk, where the AFD phase transition from the cubic to tetragonal structures occurs sharply at ~105 K, the similar structural transformation on a surface extends from 70 to 120 K. This indicates that the surface phase transitions, at least those extending into the bulk, are not localized in temperature but propagate gradually deeper into a crystal as the temperature changes.

The other two anomalies observed are brand new, solely related to surface layers and have not been observed before. Thus, there was a rather noticeable anomaly about 150 K, which is also

manifested in the growth of the lattice parameter, and involves mainly the first two surface layers (and only partially affected the third layer), which is close in parameters to the bulk spatial symmetry. This transformation is mainly local that indicates the possibility of a two–dimensional phase transition at a surface at these temperatures. At temperatures between 200 and 300 K, an additional transformation was also observed and also occured only in the first two layers and practically did not affect the third one. It may be assumed to be due to the inhibition or acceleration of the rotation of TiO_6 octahedra about the axes normal to the surface. The effect of the incommensurability between the surface lattice and the lower crystalline layers is possible as well. The tilting of the octahedron axes to the surface and variations of oxygen stoichiometry should not be also excluded.

The differentiation of the lattice parameters depending on the depth of electron penetration into the crystal revealed the nonmonotonic nature of the changes of these parameters that may be explained at least partly by the competition of contributions of TiO_2 and SrO layers. In the first one–two surface layers two possibilities are realized, i.e. the maximum or minimum value of the lattice parameters is reached. Minimum values are attained at temperatures where structural transformations are not observed. In the temperature regions, which correspond to the active structural transformations, the lattice parameters in the first one or two surface layers reach maximum values that can be considered as an indicator of a structural transformation in general. Thus such observations could be used as a method of detecting structural transformation.

The elucidation of the nature of all the anomalies identified in this work requires further experimental studies and relevant theoretical considerations such as in Refs. [30–36]. The information obtained is necessary to attain the comprehensive joint experimental and theoretical detailed understanding of the structural properties of ABO_3 perovskite surfaces in order to increase their efficiency in microelectronics and catalysis, especially at reduced temperatures. The detailed study of the low temperature surface structure and reconstruction in STO is important to clarify the nature of the revealed effects on the border of metallic ferromagnetism in similar materials.

This work was supported by the Ministry of Education and Science of Ukraine under the contract M/51–2019 within the framework of the Program of Ukrainian–Latvian Scientific and Technical Cooperation and Latvian–Ukranian Grant LV-UA/2018/2. Authors are indebted to L.L. Rusevich, G. Zvejnieks, V.P. Gnezdilov and A. Glamazda for stimulating discussions.

References

1. K.A. Muller and H. Burkard, *Phys. Rev. B.* **19**, 3593 (1979).

2. J.L. Servoin, Y. Luspin, and F. Gervais, *Phys. Rev. B* **22**, 5501 (1980).

3. K. Kamarás, K.-L. Barth, F. Keilmann, R. Henn, M. Reedyk, C. Thomsen, and M. Cardona, *J. Appl. Phys*. **78**, 1235 (1995).

4. J. Petzelt, T. Ostapchuk, I. Gregora et al., *Phys. Rev. B* **64**, 184111 (2001).

5. W.–W. Peng, R. Tétot, G. Niu, E. Amzallag, B. Vilquin, J.-B. Brubach, and P. Roy, *Sci. Rep.* **7**, 2160 (2017).

6. N. Bickel, G. Schmidt, K. Heinz, and K. Müller, *Phys. Rev. Lett.* **62**, 2009 (1989).

7. T. Hikita, T. Hanada, M. Kudo, and M. Kawai, *Surf. Sci*. **287–288**, 377 (1993).

8. M. Saghayezhian, S.M. Rezaei Sani, J. Zhang, and E.W. Plummer, *J. Phys. Chem.* C **123**, 8086 (2019).

9. R. Khachaturyan, J. Wehner, and Y.A. Genenko, *Phys. Rev. B* **96**, 054113 (2017).

10. R. Khachaturyan and Y.A. Genenko, *Phys. Rev. B* **98**, 134106 (2018).

11. Y.A. Genenko, R. Khachaturyan, J. Schultheiß, A. Ossipov, J.E. Daniels, and J. Koruza, *Phys. Rev. B* **97**, 144101 (2018).

12. H. Unoki and T. Sakudo, *J. Phys. Soc. Jpn.* **23**, 546 (1967).

13. L. Rimai and G.A. deMars, *Phys. Rev.* **127**, 702 (1962).

14. G. Shirane and Y. Yamada, *Phys. Rev.* **177**, 858 (1969).

15. A.D. Bruce and R.A. Cowley, Structural Phase Transitions, Taylor & Francis, London, 1981.

16. F.W. Lytle, *J. Appl. Phys*. **35**, 2212 (1964).

17. A.V. Kityk, W. Schranz, P. Sondergeld, D. Havlik, E.K.H.Salje, and J.F. Scott, *Phys. Rev. B* **61**, 946 (2000).

18. C. Ang, J.F. Scott, Z. Yu, H. Ledbetter, and J.L. Baptista, *Phys. Rev. B* **59**, 6661 (1999).

19. R. Vacher, J. Pelous, B. Hennion, G. Coddens, E. Courtens, and K.A. Müller, *Europhys. Lett*. **17**, 45 (1992).

20. O.-M. Nes, K.A. Müller, T. Suzuki, and F. Fossheim, *Europhys. Lett.* **19**, 397 (1992).

21. K.A. Müller, *Phys. Rev. Lett*. **2**, 341 (1959).

22. P.A. Fleury, J.F. Scott, and J.M. Worlock, *Phys. Rev. Lett*. **21**, 16 (1968).

23. J.F. Scott, *Rev. Mod. Phys*. **46**, 83 (1974).

24. G. Shirane, *Rev. Mod. Phys*. **46**, 437 (1974).

25. H. Thomas and K.A. Müller, *Phys. Rev. Lett*. **21**, 1256 (1968).

26. A. Migliori, J.L. Sarrao, W.M. Visscher, T.M. Bell, M. Lei, Z. Fisk, and R.G. Leisure, *Physica B* **183**, 1 (1993).

27. C.N.W. Darlington and D.A. Q'Connor, *J. Phys. C: Solid State Phys*. **9**, 3561 (1976).

28. J. Prade, U. Schröder, W. Kress, F.W. de Wette, and A.D. Kulkarni, *J. Phys.: Condens. Matter* **5** , 1 (1993).

29. A. Dejneka, V. Trepakov, and L. Jastrabik, *Phys. Stat. Solidi* B **247**, 1951 (2010).

30. E. Heifets, E.A. Kotomin, V. Trepakov, *J. Phys: Cond. Matter*, **18**, 4845 (2006).

31. S. Piskunov, E.A. Kotomin, E. Heifets, J. Maier, R.I. Eglitis, and G. Borstel, *Surf. Sci*. **575**, 75 (2005).

32. E. Heifets, R.I. Eglitis, E.A. Kotomin, J. Maier, and G. Borstel, *Phys. Rev. B* **64**, 235417 (2001).

33. E. Heifets, S. Dorfman, D. Fuks, E.A. Kotomin, A. Gordon, *J. Phys:Cond. Matter*,**10**, L347 (1998).

34. E. Blokhin, R.A. Evarestov, D. Gryaznov, E.A. Kotomin, and J. Maier, *Phys. Rev. B* **88**, 241407(R) (2013).

35. R.A. Evarestov, E. Blokhin, D. Gryaznov, E.A. Kotomin, and J. Maier, *Phys. Rev. B* **83**, 134108 (2011).

36. E.A. Kotomin, R.I. Eglitis, J. Maier, and E. Heifets, *Thin Solid Films* **400**, 76 (2001).

37. M. Naito and H. Sato, *Physica C* **229**, 1 (1994).

38. L. Gu, H. Wei, Z. Peng, and H. Wu, *J. Mater. Res. V* **32**, 748 (2017).

39. J. Petzelt, T. Ostapchuk, I. Gregora, I. Rychetsky´, S. Hoffmann-Eifert, A. V. Pronin, et al., *Phys. Rev. B* **64**, 184111 (2001).

40. Yu. I. Yuzyuk, *Fiz. Tverd. Tela* **54**, 963 (2012) [*Phys. Sol. State* **54**, 1026 (2012)].

41. D.J. Gray Jr., T.A. Merz, Y. Hikita, H.Y. Hwang, H. Mabuchi, *Phys. Rev. B* **94**, 214107 (2016).

42. N.V. Krainyukova and V.V. Butskii, *Surf. Sci*. **454–456**, 628 (2000).

43. N.V. Krainyukova and V.V. Butskii, *Appl. Surf. Sci*. **235**, 43 (2004).

44. M. Arrigoni, T.S. Bjørheim, E. Kotomin, and J. Maier, *Phys. Chem. Chem. Phys.* **18**, 9902 (2016).

45. S.E. Rowley, L.J. Spalek, R.P. Smith, M.P.M. Dean, M. Itoh, J.F. Scott, G.G. Lonzarich, and S.S. Saxena, *Nature Physics* **10**, 367 (2014).

46. M. Arrigoni, E.A. Kotomin, J. Maier, *Isr. J. Chemistry* **57**, 509 (2017).

47. A.A. Sirenko, C. Bernhard, A. Golnik, A.M. Clark, J. Hao, W. Si, and X.X. Xi, *Nature* **404**, 373 (2000).

48. C. Song, X. Li, Y. Jiang, X. Wang, J. Yao, S. Meng, and J. Zhang, *ACS Appl. Mat. & Interf.* **11**, 37279 (2019).

Institute of Solid State Physics, University of Latvia as the Center of Excellence has received funding from the European Union's Horizon 2020 Framework Programme H2020-WIDESPREAD-01-2016-2017-TeamingPhase2 under grant agreement No. 739508, project CAMART²